JCB Article

Inducible dimerization of FGFR1: development of a mouse model to analyze progressive transformation of the mammary gland

Bryan E. Welm,[1,2] Kevin W. Freeman,[2,3] Mercy Chen,[1] Alejandro Contreras,[1] David M. Spencer,[2,3] and Jeffrey M. Rosen[1,2]

[1]Department of Molecular and Cellular Biology, [2]Program in Cell and Molecular Biology, and [3]Department of Immunology, Baylor College of Medicine, Houston, TX 77030

To develop an inducible and progressive model of mammary gland tumorigenesis, transgenic mice were generated with a mouse mammary tumor virus–long terminal repeat–driven, conditional, fibroblast growth factor (FGF)–independent FGF receptor (FGFR)1 (iFGFR1) that can be induced to dimerize with the drug AP20187. Treatment of transgenic mice with AP20187 resulted in iFGFR1 tyrosine phosphorylation, increased proliferation, activation of mitogen-activated protein kinase and Akt, and lateral budding. Lateral buds appeared as early as 3 d after AP20187 treatment and initially consisted of bilayered epithelial cells and displayed apical and basolateral polarity appeared after 13 d of AP20187 treatment. Invasive lesions characterized by multicell-layered lateral buds, decreased myoepithelium, increased vascular branching, and loss of cell polarity were observed after 2–4 wk of treatment. These data indicate that acute iFGFR1 signaling results in increased lateral budding of the mammary ductal epithelium, and that sustained activation induces alveolar hyperplasia and invasive lesions.

Introduction

The fibroblast growth factor (FGF)* family consists of >20 ligands and four receptor tyrosine kinase genes that have been shown to be important regulators of angiogenesis and embryonic organogenesis (Ornitz, 2000). Loss-of-function experiments have demonstrated that FGFs are critical factors for limb bud outgrowth, lung development, gastrulation, and brain development (Lewandoski et al., 2000). In the adult, aberrant regulation of FGF ligands and their receptors is associated with breast and prostate tumorigenesis (Giri et al., 1999; Valve et al., 2001). Therefore, understanding the function of FGFs and FGF receptors (FGFRs) will be a crucial step in elucidating mechanisms of cellular transformation.

The expression of FGF ligands and FGFRs is developmentally regulated in the mammary gland (Coleman-Krnacik and Rosen, 1994; Chodosh et al., 2000), where they are generally expressed during ductal morphogenesis and decrease throughout pregnancy and lactation. Ductal morphogenesis is a highly proliferative stage during mammary gland development, during which the gland invades the stromal fat pad and establishes a branched ductal network (Williams and Daniel, 1983). FGFR1 is mainly expressed during this stage of development (Chodosh et al., 2000). Additionally, expression of a dominant negative FGFR2 in the mammary gland during pregnancy has been shown to inhibit lobuloalveolar development (Jackson et al., 1997). This expression profile suggests that FGF signaling plays an important role in normal mammary gland development.

The observation that mouse mammary tumor virus (MMTV) proviral insertion can activate FGF-3, FGF-4, and FGF-8 and leads to mammary tumorigenesis has revealed that FGF ligands are potent mammary gland mitogens (van Leeuwen and Nusse, 1995). The direct transforming activity of the same FGFs in the mammary gland was subsequently

The online version of this article contains supplemental material.

Address correspondence to J.M. Rosen, Dept. of Molecular and Cellular Biology, Baylor College of Medicine, One Baylor Plaza, Houston, TX 77030. Tel.: 713-798-6210. Fax: 713-798-8012.
E-mail: jrosen@faculty.bcm.tmc.edu

B.E. Welm's present address is Dept. of Anatomy, University of California, San Francisco, San Francisco, CA 94143.

*Abbreviations used in this paper: BrdU, 5-bromo-2′-deoxyuridine; ECM, extracellular matrix; FGF, fibroblast growth factor; FGFR, FGF receptor; H&E, hematoxylin and eosin; HA, hemagglutinin; LTR, long terminal repeat; MAPK, mitogen-activated protein kinase; MMP, matrix metalloproteinase; MMTV, mouse mammary tumor virus; PR, progesterone receptor; TEB, terminal-end bud; TUNEL, TdT-mediated dUTP-biotin nick end labeling.

Key words: breast cancer; FGFR; inducible dimerization; mammary gland development; angiogenesis

confirmed using transgenic mouse models (Daphna-Iken et al., 1998). Additionally, inappropriate regulation of FGFs and their receptors has been observed in breast cancer cell lines and in ~10–20% of primary breast tumors (Penault-Llorca et al., 1995; Marsh et al., 1999). These data suggest that aberrant FGF signaling may exert potent transforming capacity in the mammary gland.

In the present study, the effects of FGFR1 signaling have been investigated using a novel, inducible FGFR oligomerization and activation system. This system was first characterized in fibroblasts and mammary epithelial cells, and then in a transgenic mouse model. Inducible iFGFR1 signaling in mammary epithelium resulted in progressively invasive lesions occurring rapidly within 2–4 wk after iFGFR1 activation. iFGFR1 kinase-induced lesions were examined for cell polarity, hormonal dependence, and invasive properties. This work describes the first application of an inducible dimerization system for studying receptor tyrosine kinase signaling in a transgenic mouse model.

Results

Generation of an inducible iFGFR1 construct

A ligand-independent activation system of the FGFR was employed to study the progressive steps of mammary gland transformation. This system is based on the ability of the FK506 binding protein-12 (FKBP12) to interact with its naturally occurring ligand, FK506 (Spencer et al., 1993; Pruschy et al., 1994). The interaction of FKBP12 with FK506 occurs at a stochiometry of 1:1; thus, the tethering of two FK506 compounds results in a bivalent drug (FK1012) with the capacity to interact with and dimerize two FKBP12 containing proteins. This system has been used to study dimerization-induced signaling by several cell surface receptors, including members of the ErbB family of receptor tyrosine kinases and the T-cell receptor, as well as by intracellular proteins such as caspases (Spencer et al., 1993; Fan et al., 1999; Muthuswamy et al., 1999, 2001). Using this strategy, chimeric proteins that contain the FGFR kinase domain fused to FKBP12 can be induced to dimerize in the presence of FK1012. A synthetic analogue of FK1012 used in the present studies, AP20187, has been modified to reduce interactions with endogenous FKBPs, and specifically interacts with a variant of FKBP12 containing an F36V mutation (Clackson et al., 1998; Yang et al., 2000). The FGFR–FKBPv fusion proteins (iFGFRs) generated in this study lack the extracellular ligand binding and transmembrane domains, contain an NH_2-terminal myristylation sequence, an intracellular FGFR kinase domain, two FKBPv domains, and a COOH-terminal hemagglutinin (HA) epitope sequence (Fig. 1 A). The FGFR1 kinase domain used to generate the iFGFR1 construct contains the intracellular domain of FGFR1 (amino acids 365–822, EMBL/GenBank/DDBJ accession no. U22324) starting three amino acids from the end of the transmembrane domain. Although all four FGFRs were subcloned with the FKBPv domains, only the results obtained with iFGFR1 will be described in detail. A control FKBPv construct also was designed that contains all of the above domains except the FGFR sequences.

AP20187-dependent activation of iFGFR1 signaling in NIH3T3 fibroblasts and HC11 mammary epithelial cells

The phosphorylation levels of iFGFR1, mitogen-activated protein kinase (MAPK), and Akt were determined in both NIH3T3 and HC11 cells transduced with retroviral expression constructs to examine the downstream effects of iFGFR1 dimerization (Fig. 1, A and B). An increase in the tyrosine phosphorylation of iFGFR1 was rapidly detected after AP20187 treatment of iFGFR1-transduced NIH3T3 cells, as determined by immunoprecipitation and immunoblotting using phosphotyrosine and HA epitope antibodies, respectively (Fig. 1 B). Phosphorylation of both MAPK and Akt was also detected in AP20187-treated NIH3T3 fibroblasts and HC11 mammary epithelial cells (Fig. 1 C). Similar results were obtained with placement of the FKPBv domain NH_2-terminal to the FGFR1 kinase domain (unpublished data). No increase in MAPK or Akt phosphorylation was observed with cells transduced with FKBPv alone and treated with AP20187 (unpublished data). FGF signaling has been shown to specifically induce tyrosine phosphorylation of the 90-kD adapter protein FRS2/SNT. The tyrosine phosphorylation of FRS2/SNT was examined in AP20187-treated iFGFR1-transduced NIH3T3 fibroblasts to determine if iFGFR1 activation can signal through this pathway. FRS2/SNT was observed to be highly tyrosine phosphorylated in response to AP20187 treatment (Fig. 1 D), demonstrating that iFGFR1 signaling can activate physiological FGF signaling pathways.

The iFGFR1 and FKBPv constructs were tested in both the fibroblast and mammary epithelial cell lines to determine if they could functionally recapitulate effects mediated by FGF signaling in an AP20187-dependent fashion. One characteristic of NIH3T3 fibroblasts is their dependence on serum growth factors for survival and proliferation. iFGFR1 and FKPBv stably transfected NIH3T3 cells were plated in duplicate plates, grown to subconfluence, placed in serum-free media containing either 30 pM AP20187 or vehicle alone, and then observed for morphological changes over a 72-h time course. When grown in serum-free media in the absence of AP20187, iFGFR1 cells displayed distinct morphological features associated with apoptosis, including membrane blebbing, rounding, and detachment from the surface of the cell culture dish (Fig. 1 E, iFGFR1−; unpublished data). Similar results were obtained with the pBK-neo and FKBPv stably transfected cells in serum-free media treated with and without AP20187 (Fig. 1 E, pBKneo−, pBKneo+; unpublished data). However, iFGFR1 cells treated with AP20187 in the absence of serum remained attached to the cell culture dish, formed distinct multicellular foci and did not display morphological features characteristic of apoptosis (Fig. 1 E, iFGFR1+). A twofold increase in the number of viable cells was observed 48 h after treatment with AP20187 as determined by bioreduction of MTS (Fig. 1 E, iFGFR+). These changes were similar to those observed after treatment of NIH3T3 cells with recombinant FGF-8 under the same serum-free conditions (Fig. 1 F, rFGF8). Thus, treatment of cells stably transfected with iFGFR1 with AP20187 induced a survival response and prevented the contact inhibition that is normally observed in NIH3T3 cells.

Caspase-3 activation was assayed in serum-starved, iFGFR1-transduced NIH3T3 cells in the presence or ab-

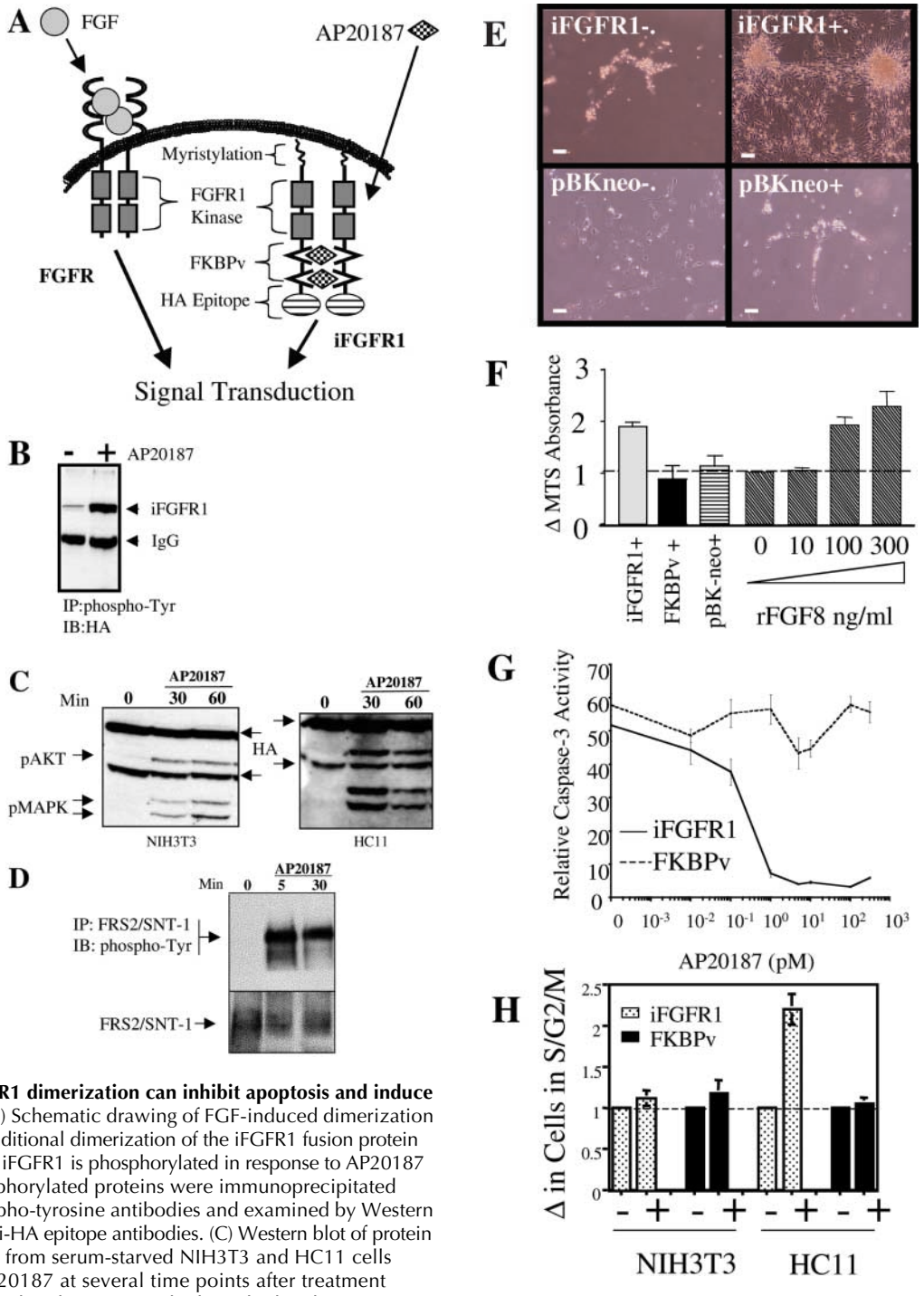

Figure 1. **iFGFR1 dimerization can inhibit apoptosis and induce proliferation.** (A) Schematic drawing of FGF-induced dimerization of FGFR and conditional dimerization of the iFGFR1 fusion protein by AP20187. (B) iFGFR1 is phosphorylated in response to AP20187 treatment. Phosphorylated proteins were immunoprecipitated using anti–phospho-tyrosine antibodies and examined by Western analysis with anti-HA epitope antibodies. (C) Western blot of protein extracts isolated from serum-starved NIH3T3 and HC11 cells treated with AP20187 at several time points after treatment (in minutes). Anti–phospho-MAPK and -Akt antibodies show activation of these kinases in response to AP20187 treatment. (D) FRS2/SNT was immunoprecipitated using anti-FRS2 antibodies and tyrosine phosphorylation was analyzed by immunoblotting with anti–phospho-tyrosine antibodies (top). Equal loading of protein on the blot was determined by reprobing the membrane with anti-FRS2 antibodies (bottom). (E) Survival assays were performed using serum-starved NIH3T3 cells. iFGFR1 cells were stably transfected with iFGFR1, whereas pBKneo cells were stably transfected with pBKneo neomycin selection cassette. iFGFR1+ and pBKneo+ cells were treated with 30 pM AP20187, whereas iFGFR1− and pBKneo− cells were treated with ethanol solvent. iFGFR1+ cells remained viable when serum starved. (F) The change in cell number from survival assays was quantitated by MTS bioreduction. The fold-change in cell number was determined by normalizing to the untreated control (−AP20187 or without rFGF8) for each condition. (G) Caspase-3 fluorometric peptide cleavage assay of serum-starved NIH3T3 cells transduced with iFGFR1 or FKBPv alone and treated with increasing concentrations of AP20187. AP20187-treated iFGFR1 cells showed reduced caspase-3 activity when compared with FKBPv control cells. Data points represent quadruplicate wells. (H) Fold difference in proliferation of AP20187-treated serum-starved NIH3T3 and HC11 cells. Spotted bars represent iFGFR1 and solid black bars FKBPv controls. Data were normalized to cells treated with solvent. Proliferating cells were determined by >2 N DNA content as measured by propidium iodide staining and FACS analysis. Only iFGFR1-transduced HC11 cells showed an increase in proliferation in response to AP20187. Data points represent at least three independent analyses. Error bars represent standard error of the mean. Bars, 5 μm.

sence of AP20187 to quantitate the iFGFR1-induced inhibition of apoptosis (Fig. 1 G). Cells were placed in serum-free medium with or without AP20187 for 24 h. Under these conditions, a significant dose-dependent decrease in caspase-3 activity was detected beginning with a dose of 0.5 pM AP20187 (Fig. 1 G, solid line). A maximal decrease was achieved with 30 pM AP20187. No significant decrease in caspase-3 activity was detected using the control FKBPv construct (Fig. 1 G, dashed line). An AP20187-dependent increase in mRNA for the antiapoptotic factor Bcl-xl was also observed (unpublished data). These data suggest that iFGFR1 activation can inhibit caspase-3–mediated apoptosis caused by serum withdrawal.

Cell cycle analysis was employed in these two different cell types to determine if the AP20187-induced iFGFR1 signaling pathway also regulates proliferation. Transduced NIH3T3 fibroblasts and HC11 mammary epithelial cells were treated with AP20187 in serum-free media and cellular DNA content was quantitated by propidium iodide staining and FACS (Fig. 1 H). NIH3T3 cells expressing iFGFR1 showed no change in proliferation with or without AP20187. However, HC11 cells expressing iFGFR1 showed greater than a twofold increase in proliferation in response to AP20187. In the presence or absence of AP20187, no difference in proliferation was detected in the control FKBPv transduced HC11 or NIH3T3 cells (Fig. 1 H, black bars). These data suggest that iFGFR1-regulated signaling pathways may exert functionally different effects that are cell type dependent. Although iFGFR1 appears to activate the same downstream pathways in fibroblasts and mammary epithelial cells, effects on their proliferation are not equivalent.

Generation of MMTV iFGFR1 transgenic mice

Transgenic mice were generated that express the iFGFR1 construct under the control of the MMTV long-terminal repeat (LTR). iFGFR1 and iFGFR2 constructs were subcloned into an MMTV transgene cassette for the generation of transgenic mice (Leder et al., 1986). Three iFGFR1 and four FGFR2-FKBPv lines were generated that transmitted the transgene through the germline. Of these seven lines, three (one iFGFR1 and two iFGFR2) expressed the transgene in the mammary gland as detected by Western blot analysis of the HA epitope tag (unpublished data). All three expressing lines displayed normal morphology in virgin mice and similar inducible phenotypes described below. A detailed characterization was performed on the iFGFR1 line 4775, which expressed low levels of iFGFR1 mRNA, detectable by RT-PCR, and low levels of protein expression as determined by Western blot analysis (unpublished data).

Activation of iFGFR1 results in increased lateral buds

To analyze the ductal morphology of mammary glands in the expressing transgenic lines, whole-mount analysis of the thoracic and inguinal glands was performed. 6-wk-old transgenic and control mice were treated intraperitoneally with injections (50 μg at 0.5 mg ml^{-1}) of AP20187 every 3 d for 16 d, or by intrascapular implantation of Alzet minipumps containing 100 μl of 0.5 mg ml^{-1} AP20187 which delivered 0.25 μl h^{-1} for 2 wk. After AP20187 treatment, the inguinal mammary glands were biopsied for whole-mount and immunofluorescence analyses (Fig. 2). Whole-mount analysis of the mammary epithelium showed no gross morphological differences between age-matched nontransgenic littermates treated with AP20187 and transgenic littermates treated with solvent only (Fig. 2, A–D). However, transgenic mice treated with AP20187 displayed increased lateral budding along the ductal epithelium (Fig. 2, E and F). AP20187-induced lateral budding was observed throughout the mammary gland and appeared on primary, secondary, and tertiary ductal branches. Increased lateral budding was also observed at the distal tips of the mammary epithelium (Fig. 2, E and F, arrowhead). Additionally, regional increases in ductal branching were observed in AP20187 treated transgenic mice (Fig. 2, E and F, arrows). Histological analysis revealed extensive lateral buds, with single and multicell-layered epithelium lining the ducts (Fig. 2 L). Although these lateral buds did contain lumens, many of these appeared constricted or convoluted.

AP20187-induced lateral budding does not require ovarian hormones

Transgenic mice were ovariectomized (ovex), and 2 d later were treated with AP20187 every 3 d for 16 d to determine if ovarian hormonal regulation is required for the lateral budding phenotype. Whole-mount analysis of ovex nontransgenic littermates treated with AP20187 showed constriction of ductal epithelium and a loss of terminal-end buds (TEBs), consistent with the loss of the inductive effects from the steroid hormones estrogen and progesterone (Fig. 2, G and H). However, when ovex transgenic mice were treated with AP20187, dilated ductal epithelium and large bloated structures at the distal tips of the ductal network were observed (Fig. 2, I and J, arrowheads). Regions of increased ductal branch points were also observed in ovex AP20187-treated transgenic mice (Fig. 2, I and J, arrows). The ductal network did not completely fill the fat pad in either transgenic or nontransgenic ovex mice treated with AP20187, suggesting that iFGFR1 activation cannot, by itself, rescue normal ductal elongation in the absence of ovarian hormones. However, the observation that iFGFR1-induced lateral budding occurred in the ovex background demonstrates that ovarian hormones are not required for this phenotype.

Transgene expression is localized to ductal and lateral bud epithelium

The localization of transgene expression in the mammary gland of transgenic mice was determined by immunofluorescent detection of the HA-epitope on the iFGFR1 protein. Mammary epithelial cells expressing the HA-epitope were observed in transgenic mice, but not in nontransgenic littermates (Fig. 2, M and N). Expression of the iFGFR1 protein was localized to the periphery of the cell and no nuclear staining was apparent, consistent with membrane targeting by the myristylation sequence. Transgene expression was punctate along the ductal epithelium of untreated 8-wk-old transgenic mice (unpublished data),

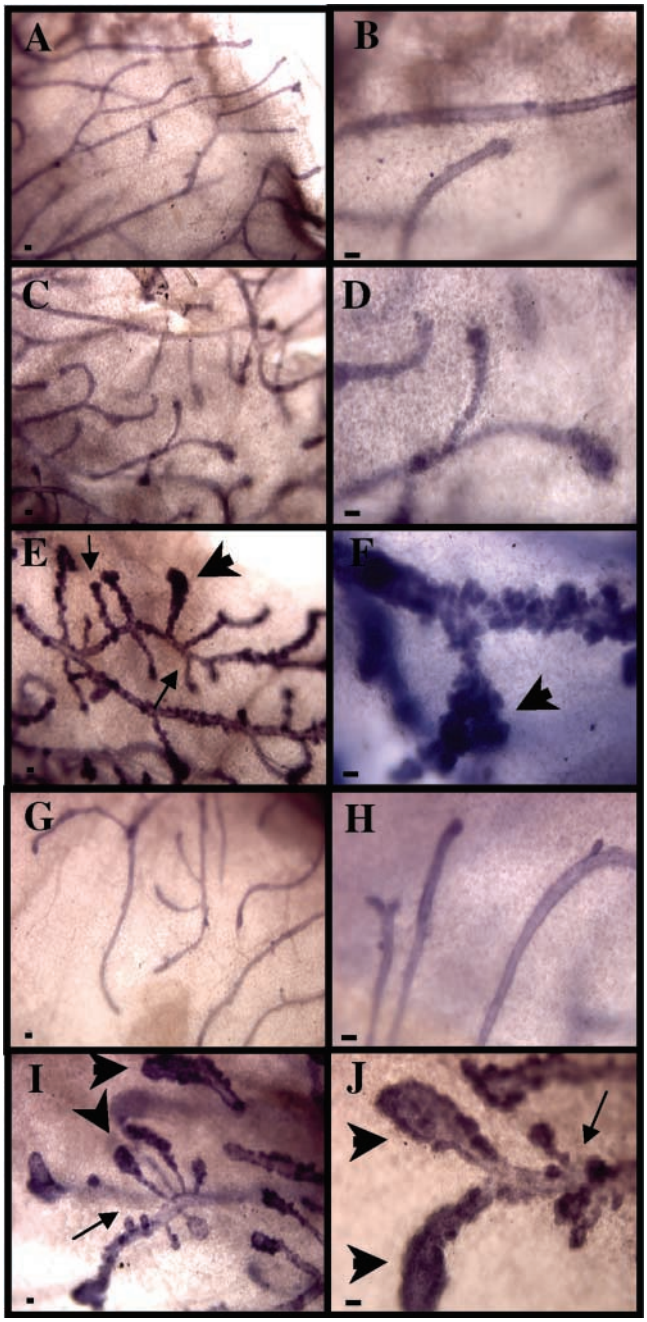

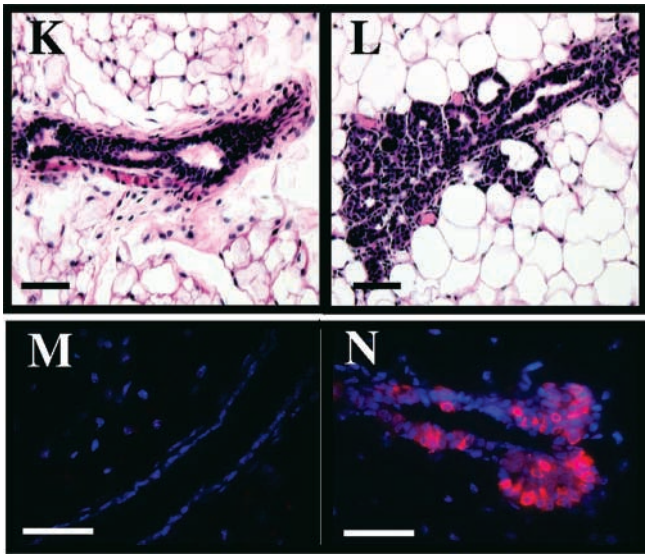

Figure 2. **iFGFR1 signaling can induce lateral buds in mammary glands of transgenic mice.** Whole-mount and histological analyses of MMTV-iFGFR1 transgenic and wild-type littermates injected i.p. with AP20187 or diluent. Whole mounts of mammary glands at 4× magnification (A, C, E, G, and I) and 10× magnification (B, D, F, H, and J). (A and B) Wild-type mouse treated with AP20187. (C and D) Transgenic mouse treated with diluent. (E and F) Transgenic mouse treated with AP20187. (G and H) Ovex wild-type mouse treated with AP20187. (I and J) Ovex transgenic mouse treated with AP20187. Arrows indicate regions of increased branching and arrowheads show lateral budding at distal regions of ducts. (K) H&E stain of transgenic mouse treated with diluent. (L) Transgenic mouse treated with AP20187. (M) Wild-type mouse stained with anti-HA antibody and Texas red secondary and DAPI-stained nuclei. (N) Transgenic mouse stained with anti-HA antibody and DAPI showing transgene localization in the lateral buds. Bars, 5 μm.

most likely due to an incomplete penetrance of the MMTV LTR-driven transgene, whereas AP20187-induced lateral buds were strongly immunoreactive (Fig. 2 N). Thus, it is possible that AP20187 treatment results in the expansion of transgene positive cells, as a result changing the expression from a punctate to a multifocal pattern. However, not all cells in lateral buds expressed the HA-tagged transgene. Instead, lateral buds contained a mixture of cell types including either transgene positive or progesterone receptor (PR)-positive cells (unpublished data). PR-positive cells within lateral buds and lining the ducts were 5-bromo-2′-deoxyuridine (BrdU) negative, consistent with the observed quiescent nature of PR-expressing cells in the mammary gland (unpublished data) (Seagroves et al., 2000).

Chronic activation of iFGFR1 results in progressively invasive lesions

Whole-mount, histological, and immunofluorescent analyses were utilized to characterize the progressive nature of the iFGFR1-induced lesions. To characterize these lesions morphologically, whole mounts and paraffin-embedded sections were stained with hematoxylin or hematoxylin and eosin (H&E), respectively. In addition, cell polarity was determined by indirect immunofluorescence microscopy using antibodies directed against specific, apical tight junction (ZO-1) and basal, basement membrane (laminin) markers. iFGFR1-induced lesions were classified into three morphologically distinct types. Type I lateral buds were characterized by the presence of a single layer of cubodial epithelium surrounded by myoepithelial cells, and with basally localized

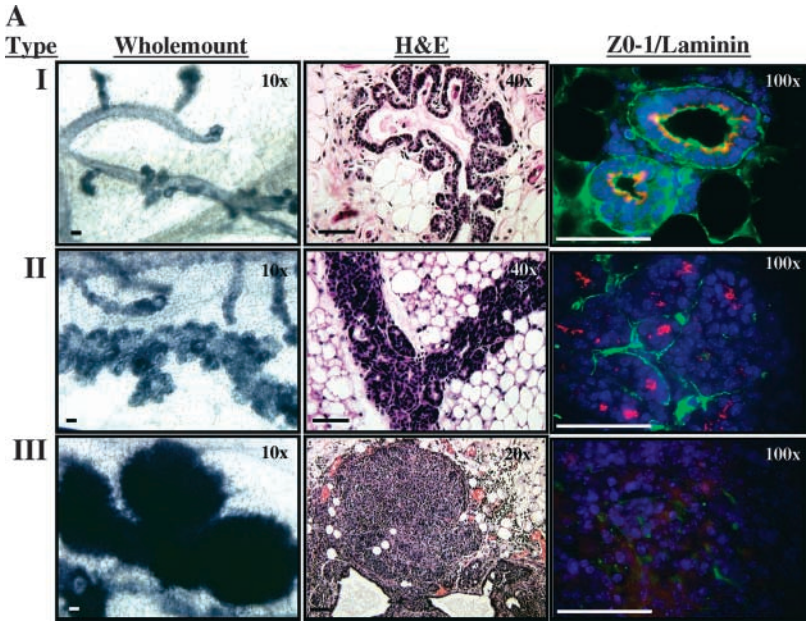

Figure 3. **Histology of iFGFR1-induced lesions in the mammary gland.** Three histologically distinct lesions are observed in AP20187-treated transgenic mouse mammary glands. (A) Panel shows gross mammary gland morphology by whole mounts (10× magnification), cellular detail by H&E stain (20 and 40×), and cellular polarity by immunofluorescence analysis (100×) with anti-ZO-1 (Texas red) and anti-laminin (FITC). Type I lesions initially appeared by day 3 of treatment, and are characterized by the punctate appearance of lateral buds lining the ductal epithelium (Type I, whole mount). Type I lateral buds contain a single layer of polarized mammary epithelial cells with large distinct lumens (Type I, H&E and ZO-1/Laminin). Type II lesions appear starting at week 2 of AP20187 treatment, and are distinguished by uniform multicellular epithelium with small collapsed lumens (Type II). Type III lesions are multicellular, invasive, well vascularized, and have lost ZO-1 and laminin expression (Type III). Bars, 5 μm.

laminin and apically localized ZO-1. Type-I lesions appeared within 3 d of AP20187 treatment and were similar to lateral alveolar buds induced in early pregnancy (Fig. 3 A, type I) (Daniel and Silberstein, 1987). However, unlike lobuloalveolar development during late pregnancy, the iFGFR1-induced lateral buds remained closely associated with their primary ducts and did not completely occupy the interductal stroma.

After ~2 wk of iFGFR1 activation, multibud, type II lesions appeared along the primary duct. These were the predominant morphology observed in the mammary gland of AP20187 treated transgenic mice (Fig. 3 A, type II). Type II lesions contained multiple cell layers and had collapsed lumens (as determined by ZO-1 localization) (Fig. 3 A). Cells at the periphery of type II lesions still remained organized around the basement membrane (as determined by anti-laminin immunofluorescent staining). Similar to type I lateral buds, these lesions remained closely associated with primary ducts, expressed PR, and were not highly invasive into the surrounding stroma (Fig. 3 A, type II; unpublished data).

Type III lesions were first observed after ~4 wk of AP20187 treatment and appeared as multifocal lesions along ducts (Fig. 3 A, type III, whole mount). Type III lesions exhibited a marked loss of laminin and ZO-1 expression, and were multicellular, invasive, and highly vascularized (Fig. 3 A, type III, H&E and immunofluorescence). These lesions were often associated with a surrounding leukocyte infiltration and reactive stroma (Fig. 3 A, type III, H&E). Interestingly, analysis of the more invasive type III lesions by FACS suggests that these lesions were predominantly diploid (unpublished data). Thus, type III lesions have some characteristics similar to intraepithelial neoplasia and thus may represent a preneoplasiac growth.

iFGFR1 dimerization induces proliferation and activation of signaling pathways in vivo

Dimerization-induced phosphorylation of the iFGFR1 protein and downstream signaling pathways were analyzed by Western blotting and immunofluorescence in transgenic mice 24 h after the completion of a 2-wk treatment with AP20187. Protein extracts isolated from AP20187-treated and -untreated transgenic littermates showed increased iFGFR1, Akt, and MAPK phosphorylation only in treated mice (Fig. 4, A and B). In transgenic mice treated for 16 d, immunolocalization of the phosphorylated (Thr202/Tyr204) MAPK correlated with the lateral bud lesions (Fig. 4, C and D). These results suggest that AP20187 treatment induced the phosphorylation and activation of the iFGFR signaling cascade in transgenic mice similar to that observed in NIH3T3 and HC11 cells.

The percentage of cells in S phase was quantitated in lateral buds as determined by BrdU incorporation to assess whether AP20187-induced lateral buds were hyperproliferative in response to activated iFGFR signaling. BrdU was administered to AP20187-treated and untreated transgenic mice 2 h before sacrifice and localized in the mammary epithelium using a FITC-conjugated anti-BrdU antibody (Fig. 4, E and F). In untreated transgenic mice, 0.9% (± 0.2 SEM) of mammary epithelial cells were positive for BrdU. However, after 28 d of AP20187 treatment, BrdU was detected in 9.5% (± 1.4 SEM) of mammary epithelial cells. The number of BrdU-positive cells found in lateral buds and ductal cells was 8.5% (± 1.6 SEM) and 11.7% (± 1.9 SEM), respectively. No significant differences were observed in apoptosis between treated and untreated transgenic mice as measured by TdT-mediated dUTP-biotin nick end labeling (TUNEL) staining (unpublished data). These results suggest that activation of the iFGFR1 kinase induces proliferation not only in regions of phenotypic lateral buds, but also within the ductal epithelium.

Transgenic mice were treated for 3 d with AP20187, followed by 120 h of drug withdrawal to assess the reversibility of the system. The half-life of AP20187 in the bloodstream has been determined previously to be ~7 h (Tim Clackson, ARIAD Pharmaceuticals, personal communication). Both the increase in MAPK phosphorylation and proliferation in the

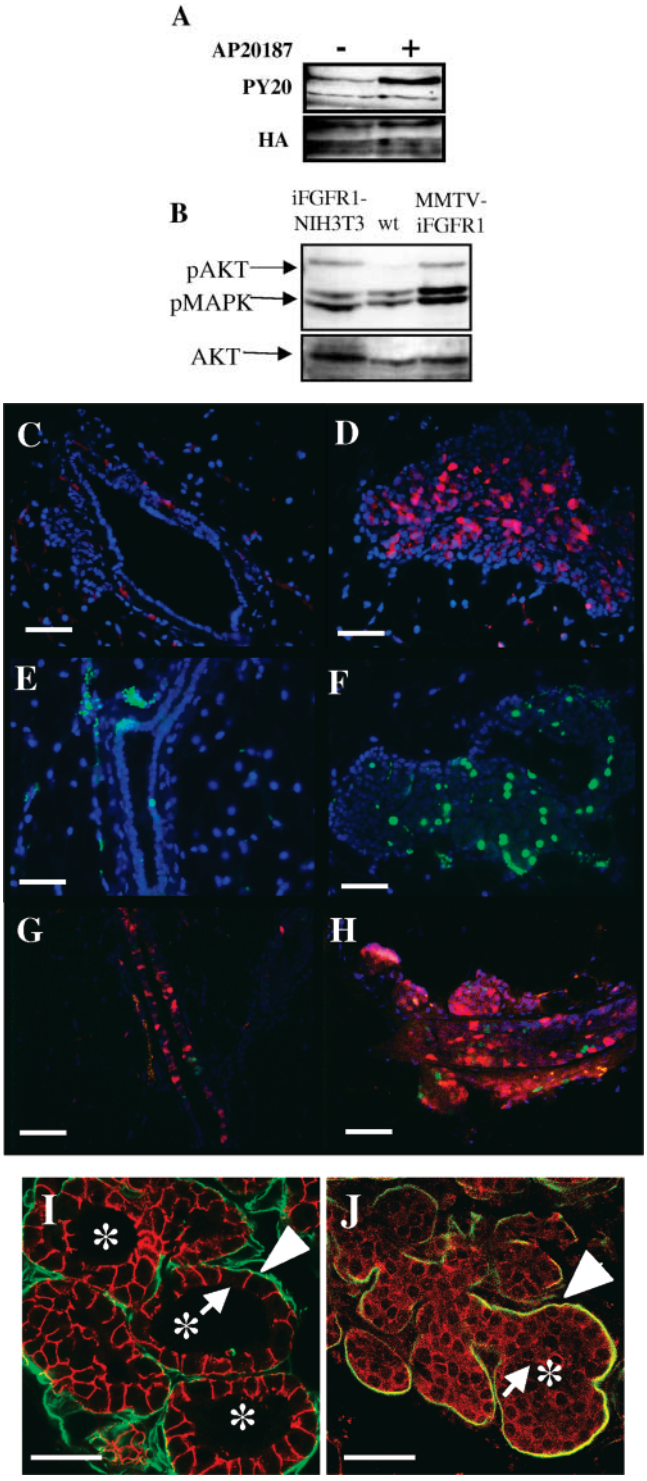

Figure 4. **AP20187 treatment of transgenic mice induces proliferation and altered cell polarity in the mammary gland.** (A) Immunoprecipitation with anti-HA epitope antibodies and Western analysis using anti–phospho-tyrosine and HA-epitope antibodies of extracts from transgenic mice treated with AP20187 (+) or diluent (−) for 2 wk. iFGFR1 shows increased phosphorylation levels in AP20187-treated transgenic mice. (B) Western blot analysis showing increased phosphorylation levels of MAPK and Akt in AP20187-treated transgenic mice (MMTV-iFGFR1) over wild-type mice treated with diluent (wt). The positive control was iFGFR1-transduced NIH3T3 cells (NIH3T3-iFGFR1) treated with AP20187. Immunofluorescence analysis with anti–phospho-MAPK antibody (Texas red) and DAPI in wild-type (C) and transgenic (D) mice treated with AP20187 for 2 wk. Anti-BrdU immunofluorescence from wild-type (E) and transgenic (F) mice treated with AP2087 for 4 wk and pulsed with BrdU for 2 h. To determine reversibility, iFGFR mice were treated for 3 d with AP20187, and treatment was stopped 120 h before tissue biopsy. Phosphorylated MAPK (Texas red) and proliferation (anti–BrdU-FITC) were detected in the AP20187-treated (G) and AP20187-withdrawal biopsy (H). Confocal microscopic and immunofluorescence analysis of midpregnant wild-type (I) and 2-wk AP20187-treated transgenic (J) mammary glands using anti–E-cadherin (Texas red, arrows) and anti-laminin (FITC, arrowhead) antibodies. AP20187-treated transgenic mice show multi-cell layering (distance between arrowhead and arrow), collapsed lumens (asterisks), and peripheral localization of E-cadherin. Bars, 5 μm.

mammary epithelium were not reversible after injections of AP20187 were stopped for 120 h before tissue biopsy (Fig. 4, G and H). Similar results were obtained when mice were treated with AP20187 for 6 wk followed by a withdrawal interval of 2 wk before to tissue biopsy (unpublished data).

iFGFR1 activation alters mammary epithelial cell polarity

Mammary epithelial cells undergo an intrinsic apoptotic response upon detachment from the basement membrane, a process termed anoikis. Confocal microscopy was utilized to determine if the iFGFR1-induced lesions contain cellular layers detached from the basement membrane. Thick frozen sections of mammary glands isolated from AP20187-treated transgenic mice were stained with anti–E-cadherin (Texas red) and laminin (FITC) antibodies (Fig. 4, I and J). Wild-type midpregnant mice were used as a control to contrast alveolar buds with iFGFR1-induced lesions. Confocal microscopic analysis showed that the mammary epithelium forms a single layer of cells contacting both the laminin-rich basement membrane (Fig. 4 I, arrowhead) and lumenal space (Fig. 4 I, asterisk) in wild-type midpregnant mice. Additionally, E-cadherin localization was observed only on lateral sides of epithelial cells, at sites of cell-to-cell contact, and not at the apical or basal membranes (Fig. 4 I, arrow). Transgenic mice treated with AP20187 formed multicellular layers with inner (lumenal) layers detached from the basement membrane (Fig. 4 J, arrow). Additionally, E-cadherin staining was observed on the entire periphery of epithelial cells, suggesting cell-to-cell contact was no longer restricted to lateral membranes (Fig. 4 J, arrow). The loss of attachment to the basement membrane and peripheral contacts with neighboring cells suggests that iFGFR1-induced lesions are no longer responsive to polarity signals, including anoikis. This is consistent with iFGFR1 signaling inhibiting apoptosis and inducing proliferation in the mammary epithelium.

iFGFR1-induced lesions have invasive characteristics

The presence of myoepithelial cells, extracellular matrix (ECM) and the vascular network were analyzed in AP20187-treated transgenic mice to assess the invasive characteristics of iFGFR1-induced lesions. The matrix metalloproteinases (MMPs) are a family of related Zn^{++} interacting proteases that are increasingly implicated in tumorigenesis (Benaud et al., 1998; John and Tuszynski, 2001). Analysis of MMP activity in conditioned media from iFGFR1-expressing mammary epithelial cells was used to determine if MMPs are regulated through iFGFR1 signaling. Using gelatin zymogra-

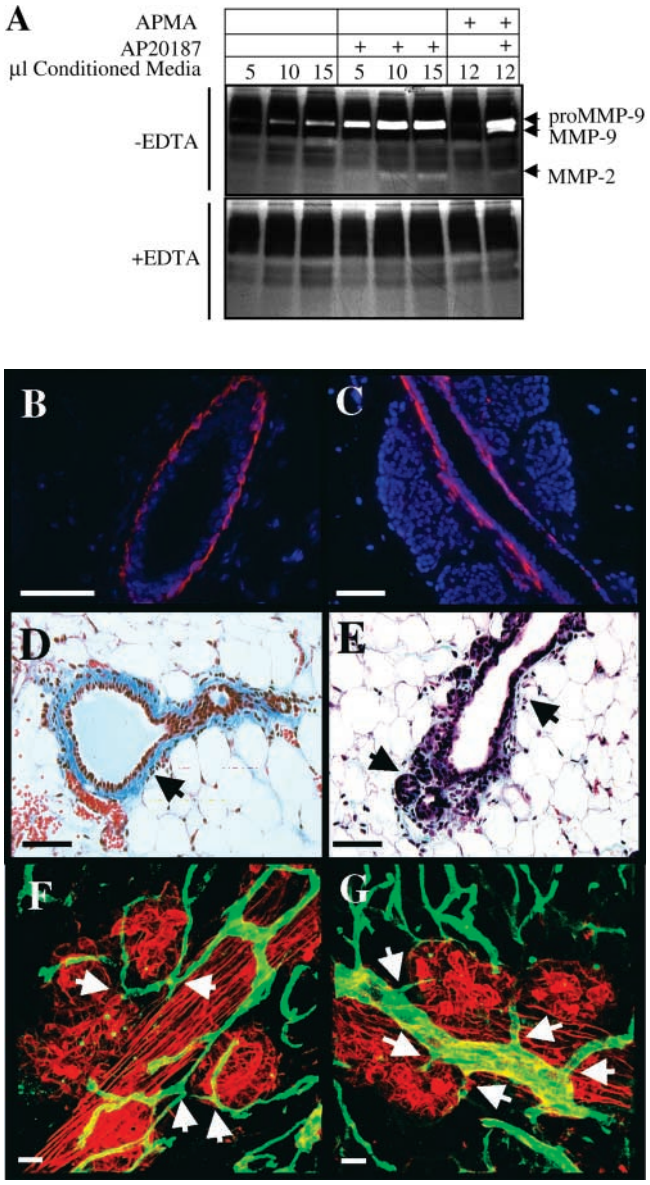

Figure 5. **iFGFR1 activation can regulate MMPs and induce invasive lesions.** (A) iFGFR-transduced HC11 cells were serum starved for 16 h and treated with AP20187 or diluent in serum-free media for 24 h. Media was collected, concentrated, and loaded in equal volumes on a gelatin zymography gel. Media isolated from AP20187-treated cells showed increased levels of MMP-9 and MMP-2 activity. APMA treatment of media for 1 h before gel loading increased the mobility of MMP-9, demonstrating conversion of proMMP-9 to active MMP-9. No APMA induced mobility shift was observed with MMP-2, suggesting only active MMP-2 was present. EDTA (5 mM) treatment in the incubation buffer inhibited MMP activity. (B and C) Indirect immunofluorescence analysis using anti-keratin-14 antibodies (Texas red) demonstrates that AP20187-treated iFGFR1 mice have reduced myoepithelium surrounding lateral buds. (D) Masson's trichrome stain of untreated transgenic mouse mammary gland epithelium showing blue stained collagen (arrow) surrounding the duct. (E) AP20187-treated mouse mammary gland with reduced collagen matrix surrounding the duct and lateral buds (arrows). (F and G) Confocal microscopy of the vascular network (FITC-lectin) surrounding the mammary epithelium (Texas red phalloidin) from AP20187-treated mice, showing increased vessel branching (arrows) associated with lateral buds. Bars, 5 µm.

phy, medium from serum-starved iFGFR1-expressing HC11 mammary epithelial cells treated with AP20187 showed increased MMP activity over solvent treated cells (Fig. 5 A). Gelatinase activity was inhibited when the chelating reagent EDTA was added to the incubation buffer (Fig. 5 A). Additionally, increased gel migration of MMP-9 was observed after pretreatment of the protein extracts with p-aminophenylmercuric acetate (APMA), an inducer of autocatalytic cleavage of proMMPs (Fig. 5 A). These data demonstrate that iFGFR1 activation in mammary epithelial cells can induce MMP-2 and MMP-9 activity.

The presence of the myoepithelial cell barrier in mammary glands from AP20187-treated mice was analyzed by confocal microscopy using antibodies against the specific myoepithelial cell markers keratin-14 (K-14) and α-actin. In untreated wild-type mice, a continuous K-14–positive cell layer was observed between the luminal epithelium and stromal cell compartments (Fig. 5 B). However, fewer K-14–positive myoepithelial cells surrounding lateral buds were observed in transgenic mice after 2 wk of AP20187 treatment. Additionally, primary ducts associated with the lateral buds displayed noncontiguous and patchy K-14 staining along the duct (Fig. 5 C). Similar results were obtained using antibodies against smooth muscle α-actin (unpublished data). The absence of myoepthelial cells correlates with a reduction of proteinaceous ECM surrounding the iFGFR1 induced lateral buds, as observed by Masson's trichrome staining (Fig. 5, D and E). However, although collagen IV (unpublished data) and laminin (Fig. 4 H) staining was still observed in the basal lamina surrounding lateral buds, their expression appeared more disorganized than in untreated mice. These data suggest that iFGFR1 activation can initiate the reorganization and breakdown of ECM surrounding the lateral buds.

Proliferation of the epithelium in the mammary gland requires concomitant changes not only in the underlying stroma, but also in the vascular network supporting the new growth. The vascular network surrounding iFGFR1-induced lateral buds was observed in situ using confocal microscopy and FITC-lectin visualization of blood vessels. To visualize blood vessels, 2-wk AP20187-treated transgenic mice were injected into the left ventricle with FITC-*Lycopersicon esculentum* lectin. FITC-lectin–injected mice were perfused with fixative, and mammary glands were biopsied and frozen in OCT compound. Mammary glands were cryosectioned and stained with Texas red phalloidin to identify the mammary epithelium. Confocal imaging and software-rendered three-dimensional reconstitution revealed a highly branched network of blood vessels surrounding iFGFR1-induced lateral buds (Fig. 5, F and G). Lateral buds were primarily associated with small tortuous vessels branching off of larger vessels lining the ductal epithelium (Fig. 5, F and G, arrows). These data suggest that sprouting angiogenesis from the existing ductal vascular network may be initiated indirectly by iFGFR1 signaling in the mammary epithelium.

Discussion

Several mouse models of breast cancer have been developed, but the utility of these models in studying the early events in

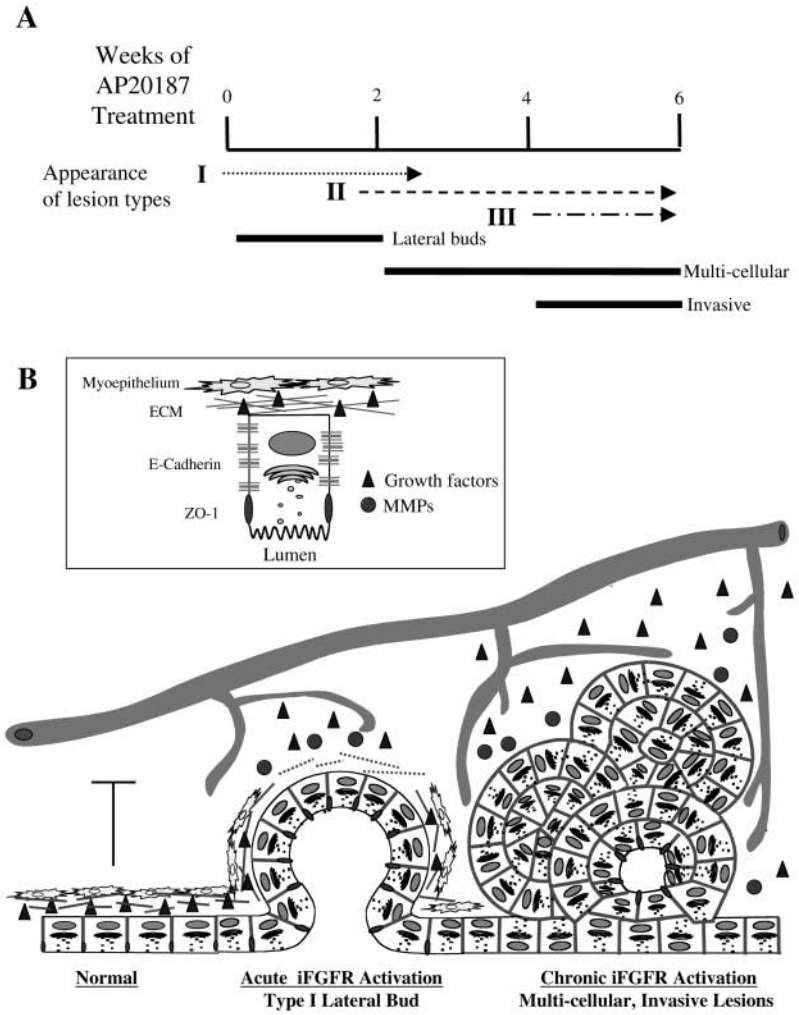

Figure 6. **Model for FGFR-induced lateral buds and hyperplasia in the mammary gland.** (A) Acute iFGFR signaling in the mammary epithelium induces lateral buds (type I) within 72 h of treatment with AP20187. Continuous treatment for 2 wk results in multicellular epithelium (type II) that can progress into invasive lesions (type III) after ~4 wk of treatment. (B) Normal mammary epithelial cells are polarized (box) with apical localization of ZO-1 at tight junctions, and lateral localization of E-cadherin. The ECM and myoepithelium at the basement membrane can regulate the bioavailability of growth factors and inhibit angiogenesis. Acute iFGFR activity in the mammary epithelium induces proliferation and upregulation of ECM proteases resulting in epithelial invasion into the stroma and the formation of lateral buds. Disruption of the ECM, through MMP upregulation (●), may induce vascular branching by increasing the bioavailability of endothelial growth factors (▲), thus supporting epithelial growth. However, chronic iFGFR activation results in disorganized cell polarity including peripheral localization of E-cadherin and loss of ZO–1 localization at tight junctions. Additionally, the loss of anti-angiogenic factors associated with the myoepithelium may contribute to the invasive characteristics of the iFGFR-induced lesions. Through these mechanisms, FGFR signaling during ductal morphogenesis may function in the proliferation and invasion of mammary epithelium to establish a ductal network, whereas its aberrant regulation may play a role in breast cancer.

transformation of the mammary gland is limited due to the inability to regulate oncogenic events. One exception to this is the use of the tetracycline-inducible system to drive expression of oncogenes in the mammary epithelium (D'Cruz et al., 2001). In this paper we describe a novel inducible mouse model of breast cancer that can be used to study the early progressive steps of tumorigenesis (Fig. 6 A). The iFGFR model is the first use of an inducible-dimerization system of a tyrosine-kinase receptor in transgenic mice.

Activation of iFGFR signaling in the mammary gland results in several distinct stages of transformation, including epithelial hyperproliferation (observable 72 h after AP20187 treatment) and stromal invasion (Fig 6 A). Several factors, including MMP regulation, ECM remodeling, and absence of a myoepithelial cell barrier, may contribute to the invasiveness of these lesions (Fig. 6 B). Myoepithelial cells play a role in the production and maintenance of the ECM barrier that surrounds ductal epithelium, and secrete antiangiogenic factors (Xiao et al., 1999; Nguyen et al., 2000). Loss of myoepithelium and ECM is associated with invasive characteristics in breast cancer (Batsakis and el-Naggar, 1999; Xiao et al., 1999). Moreover, the ECM has been implicated in an active role in the regulation of proliferation, differentiation, and angiogenesis by regulating growth factor bioavailability (Coussens et al., 2000; Silberstein, 2001). Coussens et al. (2000) have demonstrated that neutrophils expressing MMP-9 induce angiogenesis by releasing VEGF from the ECM, thus increasing its availability to endothelial cells (Coussens et al., 2000). Interestingly, we have observed that conditioned media isolated from iFGFR1-transduced mammary epithelial cells treated in culture with AP20187 displayed an increased MMP-9 and MMP-2 activity. Consistent with these data, reduced ECM and increased vascular branching surrounding iFGFR-induced lesions was observed in AP20187-treated transgenic mice. However, it is likely that the invasive nature of type III lesions may be augmented by infiltration of leukocytes and increased secretion of MMP-9 (Coussens et al., 2000). Long-term treatment (3–12 mo) of transgenic mice with AP20187 will be needed to determine if the localized invasive nature of type III lesions are premalignant and can progress to adenocarcinomas with metastatic potential.

The rapid 4-wk time period from the appearance of initial type I to the invasive type III lesions suggests that iFGFR1 signaling in mammary epithelium exerts both potent proliferative and antiapoptotic effects (Fig. 6 A). However, the complex nature of iFGFR1-induced lesions, including the loss of myoepithelium and increased vascular branching, suggest that other indirect effects mediated through stromal interactions also contribute to the invasive characteristics. The conversion

of a single layer ductal epithelium to multicell layers found in type II and type III lesions suggest that iFGFR kinase activity inhibited the apoptosis that is normally associated with detachment of lumenal epithelial cells from the basement membrane. In iFGFR1-expressing mice treated with AP20187, no significant changes in apoptosis were observed by TUNEL staining when compared with untreated mice (unpublished data). Levels of apoptosis in the ductal epithelium of mature virgin mice detected by the TUNEL assay are extremely low ($<$0.1%), thus limiting the ability to detect a decrease in apoptosis (Humphreys et al., 1996; Rosfjord and Dickson, 1999). Interestingly, recent studies using an MMTV LTR-driven Tet-regulatable system have shown that after c-myc activation, there is an increase in both proliferation and apoptosis, reaching levels of $\sim$10% in the ductal epithelial cells (D'Cruz et al., 2001). Increased lateral budding and mammary hyperplasia were also observed in this transgenic model, but required a long latency during which other stochastic events, such as Kras2 activation may occur (D'Cruz et al., 2001). In contrast, iFGFR signaling can directly activate both proliferation and survival signals within mammary epithelium to rapidly induce hyperplastic lesions. Moreover, Muthuswamy et al. (1999, 2001), using the same inducible dimerization system, demonstrated that activation of ErbB2 but not ErbB1 in human mammary epithelial MCF10A cells resulted in similar changes in proliferation and a loss of cell polarity demonstrating that highly homologous receptor tyrosine kinases can induce differential effects (Muthuswamy et al., 1999, 2001). The FGF and EGF growth factor receptor families share several downstream signaling factors that may explain the similarity in the iFGFR1- and ErbB2-induced effects on mammary epithelial cells.

During branching morphogenesis of the *Drosophila* trachea and mouse lung, signaling between the epithelium and mesenchyme is essential in ductal bifurcation, and FGF ligands and FGFRs have been implicated as critical factors in this process (Metzger and Krasnow, 1999; Sekine et al., 1999). The effects of iFGFR signaling described in this study, and the pattern of FGF ligand and FGFR expression during ductal morphogenesis, are consistent with a possible role for this growth factor family in initiating branching in the mammary gland (Fig. 6 B). In this study, iFGFR1 kinase activation elicited direct effects on mammary epithelium including regulation of proliferation, apoptosis, and MMP secretion. Additional indirect effects, including ECM remodeling and vascular branching, may function in restructuring the stroma to provide support for the developing ductal network (Fig. 6 B). Factors initiating branching morphogenesis and lateral budding should induce similar effects during mammary gland development. Therefore, it is likely that coordinated FGF signaling during ductal morphogenesis contributes to this developmental process. Conditional FGFR knockouts will be important to further substantiate the importance of FGF function during mammary gland development.

Because transgene expression levels may contribute to AP20187-independent dimerization of the iFGFR constructs, the line used in these studies (4775) had the lowest levels of protein expression, as detected by Western blot analysis, and required RT-PCR analysis for mRNA detection (unpublished data). However, all expressing lines demonstrated AP20187-independent tumorigenesis in parous mice appearing 6–12 mo after parturition (unpublished data). It is unlikely that integration effects contribute to this phenotype, as all lines exhibit both normal mammary gland morphology in untreated virgin transgenic mice, and tumors after breeding. It is more likely that during pregnancy and lactation, transgene expression is upregulated to levels that favor AP20187-independent activation, resulting in preneoplastic lesions and leading to tumorigenesis. This is consistent with the appearance of multifocal intraepithelial neoplastic lesions in the mammary glands of untreated parous mice and the long latency for tumor development (unpublished data). However, we cannot rule out other initiating factors contributed by pregnancy, lactation, or involution that may cooperate with iFGFR1 signaling to induce tumorigenesis. The use of the MMTV-LTR promoter to drive expression of the transgene may also contribute to the lack of reversibility of the lesions through the initiation of an autoregulatory loop established upon activation of iFGFR signaling. This is consistent with the observed increase in transgene expression after only 3 d of AP20187 treatment as detected by Western blot analyses (unpublished data). Transgenic mice containing iFGFR1 regulated by a tetracycline dependent promoter crossed with mice containing the reverse tetracycline-dependent transcriptional activator under the control of the MMTV promoter (D'Cruz et al., 2001), may provide an improved model to regulate both expression levels of iFGFR1 using doxycycline and iFGFR1 activity using AP20187 resulting in a reversible system in which to study tumor progression. However, the iFGFR constructs described in our study have been shown to elicit reversible effects when expressed downstream of different promoters in transgenic and tumor cell transplantation models (unpublished data).

The iFGFR1 transgenic mice provide a mouse model for the analysis of progression from early hyperproliferative to invasive lesions in the mammary gland. These mice will be useful in defining the steps necessary for transformation. However, these data must be interpreted with the caveat that the iFGFR transgene contains several differences from the endogenous FGFR1 that may alter its activation kinetics and cellular localization. The iFGFR constructs contain only the intracellular domain of the FGFR and eliminate regulatory elements found in the extracellular and transmembrane domains (Rousseau et al., 1996; Burke et al., 1998; Wang et al., 1999). The extracellular domain of the endogenous receptor confers affinity for ligand and heparin-sulfate proteoglycans that regulate signal intensity, duration, and affect cellular response. The iFGFR constructs contain a Src myristylation sequence to anchor the receptor to the plasma membrane. Thus, it is likely that this may influence the localization of the iFGFR, and also, potentially, the duration and nature of iFGFR signaling. The examination of signaling molecules that are activated by differentially localized constructs should reveal whether basolateral versus nonlocalized expression affect the duration and specificity of RTK-induced signaling pathways. Therefore, further comparison between iFGFR and FGFR signaling will be required to assess the capacity of the AP20187/FKBPv system to completely recapitulate the endogenous signaling pathways.

Materials and methods

Plasmids and cell culture

The FGFR1 intracellular kinase domain was cloned by PCR amplification of the mouse FGFR1 cDNA plasmid pMo/FR1/IRES, a gift from David Ornitz (Washington University, St. Louis, MO) using the following primers: forward 5′-ATTATAGTCGACATGAAGAGCGGCACCAAGAAGAGC-3′ and reverse 5′-CTACTTGTCGACGCGCCGTTTGAGTCCACTGTTGG-3′. The FGFR1 kinase domain was sequenced and subcloned into pSH1/MF_v-F_{vls}-E plasmid providing an NH_2-terminal myristylation sequence, two tandem FKBPv domains (F_v-F_{vls}), and hemagglutinin epitope sequence (Fan et al., 1999). The entire iFGFR1 coding region, including the NH_2-terminal myristylation and hemagglutinin epitope sequences, was subcloned into pMMP, for retroviral transduction experiments (Riviere et al., 1995). For generating transgenic mice, the iFGFR1 coding sequence was cloned into the MMTV-KCR transgene cassette, pMKBPA, a gift from Steven Chua and Franco DeMayo (Baylor College of Medicine, Houston, TX). NIH3T3 cells were grown in growth media containing DME (GIBCO BRL), 10% bovine calf serum (JRH), and 50 μg ml^{-1} gentamicin (Sigma-Aldrich). HC11 cells were grown in growth media containing RPMI 1640 medium (RPMI) (JRH) supplemented with 10% fetal bovine serum, 10 ng/ml^{-1} EGF (Life Technologies), 5 μg ml^{-1} insulin (Sigma-Aldrich), and 50 μg ml^{-1} gentamicin. Serum starvation media for NIH3T3 and HC11 cells contained only DME or RPMI, respectively, supplemented with either 30 pM AP20187 (Ariad Pharmaceuticals) in ethanol or an equal volume of ethanol-diluent alone as control. The 293T cell growth media contained DME, 10% fetal bovine serum (Summit), and 50 μg ml^{-1} gentamicin. For cell transduction, retroviruses were packaged by cotransfecting pMMP-iFGFR1 or pMMP-FKBPv plasmids with pCLEco (Imgenex) into 293T cells using FuGene (Roche) following the manufacturer's protrocol. 48 h after transfection, retrovirus-containing 293T media was supplemented with 10 μg ml^{-1} polybrene (Sigma-Aldrich), syringe filtered using a 0.4-μm filter unit (Millipore) and 5 ml were added to 100-mm plates of HC11 or NIH3T3 target cells. The target cells with retroviral media were spun in a Marathon centrifuge at 1,800 rpm (500 g) for 30 min with a 1/3 rotation of the plate every 10 min to permit equal distribution of media over the plate.

Survival and proliferation assay

For cell survival assays, the pSH1-iFGFR1 construct was cotransfected with pBKneo into NIH3T3 cells using Fugene. Stable cells were selected by supplementing growth media with 200 μg of active G418 ml^{-1} for 3 wk. Pooled NIH3T3 cells were placed in serum-free DME media for 72 h with daily media changes for morphological analysis. Images were captured using a Sony CCD-DXC-151A camera. Caspase-3 activity was measured by cleavage of the fluorogenic substrate Ac-DEVD-AMC (PharMingen). Briefly, iFGFR1 and FKBPv-transduced NIH3T3 cells were treated with AP20187 or ethanol diluent in serum-free media for 24 h, followed by cell lysis and incubation with the fluorogenic peptide according to the manufacturer's protocol. Cell proliferation was measured, following the manufacturer's protocol, by propidium iodide (Roche) staining of AP20187 or ethanol diluent–treated cells in serum-free media for 48 h. DNA content was measured by FACS. For in vivo proliferation, a BrdU label retention assay was performed as previously described by Seagroves et al. (1998). Assays were performed in triplicate or quadruplicate and repeated at least two times. BrdU quantitation was performed by counting positive cells from at least five 40× images from two or more mice.

Western blots and zymography

The following antibodies were used for Western blot analysis: phospho-MAPK; phospho-Akt and Akt (Cell Signaling); PY20 (BD Transduction Laboratories); FRS2 (Santa Cruz Biotechnology); and HA-epitope (Santa Cruz Biotechnology). Protein extracts from cultured cells were isolated with Triton X-100 extraction buffer (150 mM NaCl, 1% Triton X-100, 1 μg ml^{-1} aprotinin, 1 μg ml^{-1} benzeamidine, 1 μg ml^{-1} antipain, 10 μg ml^{-1} soybean trypsin inhibitor, 0.25 μg ml^{-1} leupeptin, 100 μM PMSF, 100 uM NaVanadate, 1 mM NaF) and passed through a 26-G syringe five times followed by incubation on ice for 45 min. Protein extracts were quantitated by Bradford assay (Bio-Rad), and 80 μg protein was resolved by SDS-PAGE and transferred onto PVDF membranes (Millipore). Western blot analyses were followed as previously described (Seagroves et al., 1998). Chemiluminsecence was developed following manufacturer's protocol (Pierce Chemical Co.). For zymography, 1.5 ml media from AP20187 or ethanol diluent–treated HC11 cells in serum-free media for 16 h was concentrated with YM-10MW Centricon membranes following the manufacturer's protocol (Millipore), loaded in equal volumes on gelatin zymography gels, and analyzed as described by Talhouk et al. (1991).

Indirect immunofluorescence and histology

The following primary antibodies were used for indirect immunofluorescent detection of specific antigens: rabbit polyclonals were anti–keratin-14 (Convance Research Products); anti-laminin (Dako); and anti–phospho-MAPK (Cell Signaling). Rat monoclonals were anti–E-cadherin (Zymed) and anti–ZO-1 (Chemicon), and mouse monoclonals were anti–HA-epitope (Convance Research Products) and anti-BrdU (Becton Dickinson). Secondary antibodies were: anti–mouse Texas red; Texas red anti–rat; FITC anti–rabbit; and Texas red anti–rabbit (Molecular Probes). Tissue was processed and stained as previously described (Seagroves et al., 1998). For confocal microscopic analysis of frozen sections, tissue was fixed in 4% PFA/PBS for 2 h and frozen in OCT. Frozen sections were cut (50 μm) and stained overnight with primary antibody in 3%BSA/PBS. Sections were washed in PBS for 10 min and stained with secondary antibodies for 5 h. Sections were then washed for 30 min, mounted with Vectashield, and analyzed using a Zeiss 510 laser scanning confocal microscope. Whole mounts were prepared as previously described (Williams and Daniel, 1983), and images were captured using Olympus dissecting microscope and Sony video camera (#DXC-151A). H&E sections were prepared as previously described (Seagroves et al., 1998). Masson's trichrome staining was performed with Accustain Trichrome Stain following the manufacturer's protocol (Sigma-Aldrich).

FITC-lectin perfusion

Mice were implanted with Alzet minipumps (Alzet) containing 100 μl of 0.5 mg ml^{-1} AP20187, delivering 0.25 μl h^{-1} for 2 wk. Mice were anesthetized after 2 wk with Avertin followed by left ventricular injection of *Lycopersicon esculentum* FITC-lectin (Vector). After 5 min, 5 ml of 1% paraformaldehyde/0.5% gluteraldehyde/PBS was perfused followed by 5 ml of PBS. Tissue was then dissected and frozen in OCT. For confocal microscopy, thick 50-μm sections of OCT embedded tissue were cut and post-fixed in 4% PFA/PBS for 10 min at room temperature. Sections were then permeablized with 1% Triton X-100 in PBS for 10 min at room temperature, washed in PBS for 5 min, and stained for 5 h with phalloidin-Alexa594 (Molecular Probes). Sections were washed for 20 min in PBS, mounted with Vectashield, and imaged.

Online supplemental material

Supplemental videos are available at http://www.jcb.org/cgi/content/full/200107119/DC1. Video 1 shows a midpregnant mouse mammary gland consisting of a single cell layer of polarized mammary epithelium. Three-dimensional rotation of the midpregnant mammary gland demonstrates the single-cell epithelial layer between the basement membrane and lumen. Video 2 represents iFGFR1-induced lesions containing multicell-layered mammary epithelium with altered cell polarity. Confocal imaging through the iFGFR1-induced lesion demonstrates the multiple cell layers, reduced lumen size, and peripheral staining of E-cadherin observed throughout these lesions. Videos 3 and 4 show increased vascular branching surrounding iFGFR1-induced lateral buds. Confocal immunofluorescence and three-dimensional imaging of the vascular network shows the close proximity and branching of blood vessels surrounding iFGFR1-induced lateral buds.

We would like to thank J. Hsu, S. Johnson, M. Gatza, and J. Wang for their help on this project. We would also like to thank Drs. M. Inoue and M. Singh (University of California, San Francisco, San Francisco, CA) for the lectin-FITC protocol, and Dr. S. Muthuswamy for helpful discussions. We thank J. Scott for flow cytometry, L. Hopkins, A. Welm and M. Gonzalez-Rimbau for histology support, and S. Small for excellent animal handling support.

B. Welm was supported by a predoctoral fellowship from the Department of Defense Breast Cancer Research Program (DAMD17-98-1-8283). This research was supported by grant CA16303 from the National Cancer Institute.

Submitted: 27 July 2001
Revised: 22 March 2002
Accepted: 22 March 2002

References

Batsakis, J.G., and A.K. el-Naggar. 1999. Myoepithelium in salivary and mammary neoplasms is host-friendly. *Adv. Anat. Pathol.* 6:218–226.

Benaud, C., R.B. Dickson, and E.W. Thompson. 1998. Roles of the matrix metalloproteinases in mammary gland development and cancer. *Breast Cancer Res. Treat.* 50:97–116.

Burke, D., D. Wilkes, T.L. Blundell, and S. Malcolm. 1998. Fibroblast growth fac-

tor receptors: lessons from the genes. *Trends Biochem. Sci.* 23:59–62.

Chodosh, L.A., H.P. Gardner, J.V. Rajan, D.B. Stairs, S.T. Marquis, and P.A. Leder. 2000. Protein kinase expression during murine mammary development. *Dev. Biol.* 219:259–276.

Clackson, T., W. Yang, L.W. Rozamus, M. Hatada, J.F. Amara, C.T. Rollins, L.F. Stevenson, S.R. Magari, S.A. Wood, and N.L. Courage, et al. 1998. Redesigning an FKBP-ligand interface to generate chemical dimerizers with novel specificity. *Proc. Natl. Acad. Sci. USA.* 95:10437–10442.

Coleman-Krnacik, S., and J.M. Rosen. 1994. Differential temporal and spatial gene expression of fibroblast growth factor family members during mouse mammary gland development. *Mol. Endocrinol.* 8:218–229.

Coussens, L.M., C.L. Tinkle, D. Hanahan, and Z. Werb. 2000. MMP-9 supplied by bone marrow-derived cells contributes to skin carcinogenesis. *Cell.* 103: 481–490.

D'Cruz, C.M., E.J. Gunther, R.B. Boxer, J.L. Hartman, L. Sintasath, S.E. Moody, J.D. Cox, S.I. Ha, G.K. Belka, A. Golant, et al. 2001. c-MYC induces mammary tumorigenesis by means of a preferred pathway involving spontaneous Kras2 mutations. *Nat. Med.* 7:235–239.

Daniel, C.W., and G.B. Silberstein. 1987. Postnatal Development of the Rodent Mammary Gland. Plenum, New York. 3–36.

Daphna-Iken, D., D.B. Shankar, A. Lawshe, D.M. Ornitz, G.M. Shackleford, and C.A. MacArthur. 1998. MMTV-Fgf8 transgenic mice develop mammary and salivary gland neoplasia and ovarian stromal hyperplasia. *Oncogene.* 17: 2711–2717.

Fan, L., K.W. Freeman, T. Khan, E. Pham, and D.M. Spencer. 1999. Improved artificial death switches based on caspases and FADD. *Hum. Gene Ther.* 10: 2273–2285.

Giri, D., F. Ropiquet, and M. Ittmann. 1999. Alterations in expression of basic fibroblast growth factor (FGF) 2 and its receptor FGFR-1 in human prostate cancer. *Clin. Cancer Res.* 5:1063–1071.

Humphreys, R.C., M. Krajewska, S. Krnacik, R. Jaeger, H. Weiher, S. Krajewski, J.C. Reed, and J.M. Rosen. 1996. Apoptosis in the terminal endbud of the murine mammary gland: a mechanism of ductal morphogenesis. *Development.* 122:4013–4022.

Jackson, D., J. Bresnick, I. Rosewell, T. Crafton, R. Poulsom, G. Stamp, and C. Dickson. 1997. Fibroblast growth factor receptor signalling has a role in lobuloalveolar development of the mammary gland. *J. Cell Sci.* 110:1261–1268.

John, A., and G. Tuszynski. 2001. The role of matrix metalloproteinases in tumor angiogenesis and tumor metastasis. *Pathol. Oncol. Res.* 7:14–23.

Leder, A., P.K. Pattengale, A. Kuo, T.A. Stewart, and P. Leder. 1986. Consequences of widespread deregulation of the c-myc gene in transgenic mice: multiple neoplasms and normal development. *Cell.* 45:485–495.

Lewandoski, M., X. Sun, and G.R. Martin. 2000. Fgf8 signalling from the AER is essential for normal limb development. *Nat. Genet.* 26:460–463.

Marsh, S.K., G.S. Bansal, C. Zammit, R. Barnard, R. Coope, D. Roberts-Clarke, J.J. Gomm, R.C. Coombes, and C.L. Johnston. 1999. Increased expression of fibroblast growth factor 8 in human breast cancer. *Oncogene.* 18:1053–1060.

Metzger, R.J., and M.A. Krasnow. 1999. Genetic control of branching morphogenesis. *Science.* 284:1635–1639.

Muthuswamy, S.K., M. Gilman, and J.S. Brugge. 1999. Controlled dimerization of ErbB receptors provides evidence for differential signaling by homo- and heterodimers. *Mol. Cell. Biol.* 19:6845–6857.

Muthuswamy, S.K., D. Li, S. Lelievre, M.J. Bissell, and J.S. Brugge. 2001. ErbB2, but not ErbB1, reinitiates proliferation and induces luminal repopulation in epithelial acini. *Nat. Cell Biol.* 3:785–792.

Nguyen, M., M.C. Lee, J.L. Wang, J.S. Tomlinson, Z.M. Shao, M.L. Alpaugh, and S.H. Barsky. 2000. The human myoepithelial cell displays a multifaceted anti-angiogenic phenotype. *Oncogene.* 19:3449–3459.

Ornitz, D.M. 2000. FGFs, heparan sulfate and FGFRs: complex interactions essential for development. *Bioessays.* 22:108–112.

Penault-Llorca, F., F. Bertucci, J. Adelaide, P. Parc, F. Coulier, J. Jacquemier, D. Birnbaum, and O. deLapeyriere. 1995. Expression of FGF and FGF receptor genes in human breast cancer. *Int. J. Cancer.* 61:170–176.

Pruschy, M.N., D.M. Spencer, T.M. Kapoor, H. Miyake, G.R. Crabtree, and S.L. Schreiber. 1994. Mechanistic studies of a signaling pathway activated by the organic dimerizer FK1012. *Chem. Biol.* 1:163–172.

Riviere, I., K. Brose, and R.C. Mulligan. 1995. Effects of retroviral vector design on expression of human adenosine deaminase in murine bone marrow transplant recipients engrafted with genetically modified cells. *Proc. Natl. Acad. Sci. USA.* 92:6733–6737.

Rosfjord, E.C., and R.B. Dickson. 1999. Growth factors, apoptosis, and survival of mammary epithelial cells. *J. Mammary Gland Biol. Neoplasia.* 4:229–237.

Rousseau, F., J. Bonaventure, L. Legeai-Mallet, A. Pelet, J.M. Rozet, P. Maroteaux, M. Le Merrer, and A. Munnich. 1996. Mutations of the fibroblast growth factor receptor-3 gene in achondroplasia. *Horm. Res.* 45:108–110.

Seagroves, T.N., S. Krnacik, B. Raught, J. Gay, B. Burgess-Beusse, G.J. Darlington, and J.M. Rosen. 1998. C/EBPbeta, but not C/EBPalpha, is essential for ductal morphogenesis, lobuloalveolar proliferation, and functional differentiation in the mouse mammary gland. *Genes Dev.* 12:1917–1928.

Seagroves, T.N., J.P. Lydon, R.C. Hovey, B.K. Vonderhaar, and J.M. Rosen. 2000. C/EBPbeta (CCAAT/enhancer binding protein) controls cell fate determination during mammary gland development. *Mol. Endocrinol.* 14:359–368.

Sekine, K., H. Ohuchi, M. Fujiwara, M. Yamasaki, T. Yoshizawa, T. Sato, N. Yagishita, D. Matsui, Y. Koga, N. Itoh, and S. Kato. 1999. Fgf10 is essential for limb and lung formation. *Nat. Genet.* 21:138–141.

Silberstein, G.B. 2001. Postnatal mammary gland morphogenesis. *Microsc. Res. Tech.* 52:155–162.

Spencer, D.M., T.J. Wandless, S.L. Schreiber, and G.R. Crabtree. 1993. Controlling signal transduction with synthetic ligands. *Science.* 262:1019–1024.

Talhouk, R.S., J.R. Chin, E.N. Unemori, Z. Werb, and M.J. Bissell. 1991. Proteinases of the mammary gland: developmental regulation in vivo and vectorial secretion in culture. *Development.* 112:439–449.

Valve, E.M., M.T. Nevalainen, M.J. Nurmi, M.K. Laato, P.M. Martikainen, and P.L. Harkonen. 2001. Increased expression of FGF-8 isoforms and FGF receptors in human premalignant prostatic intraepithelial neoplasia lesions and prostate cancer. *Lab. Invest.* 81:815–826.

van Leeuwen, F., and R. Nusse. 1995. Oncogene activation and oncogene cooperation in MMTV-induced mouse mammary cancer. *Semin. Cancer Biol.* 6:127–133.

Wang, Y., M.K. Spatz, K. Kannan, H. Hayk, A. Avivi, M. Gorivodsky, M. Pines, A. Yayon, P. Lonai, and D. Givol. 1999. A mouse model for achondroplasia produced by targeting fibroblast growth factor receptor 3. *Proc. Natl. Acad. Sci. USA.* 96:4455–4460.

Williams, J.M., and C.W. Daniel. 1983. Mammary ductal elongation: differentiation of myoepithelium and basal lamina during branching morphogenesis. *Dev. Biol.* 97:274–290.

Xiao, G., Y.E. Liu, R. Gentz, Q.A. Sang, J. Ni, I.D. Goldberg, and Y.E. Shi. 1999. Suppression of breast cancer growth and metastasis by a serpin myoepithelium-derived serine proteinase inhibitor expressed in the mammary myoepithelial cells. *Proc. Natl. Acad. Sci. USA.* 96:3700–3705.

Yang, W., L.W. Rozamus, S. Narula, C.T. Rollins, R. Yuan, L.J. Andrade, M.K. Ram, T.B. Phillips, M.R. van Schravendijk, and D. Dalgarno, et al. 2000. Investigating protein-ligand interactions with a mutant FKBP possessing a designed specificity pocket. *J. Med. Chem.* 43:1135–1142.